THE JOURNAL OF BIOLOGICAL CHEMISTRY VOL. 283, NO. 24, pp. 16561–16572, June 13, 2008

Functional Interaction between Paramyxovirus Fusion and Attachment Proteins*[S]

Received for publication, February 7, 2008, and in revised form, April 16, 2008 Published, JBC Papers in Press, April 21, 2008, DOI 10.1074/jbc.M801018200

Jin K. Lee[‡], Andrew Prussia[§], Tanja Paal[‡], Laura K. White[‡], James P. Snyder[§], and Richard K. Plemper[‡1]

From the [‡]Department of Pediatrics, Emory University School of Medicine and the [§]Department of Chemistry, Emory University, Atlanta, Georgia 30322

Paramyxovirinae envelope glycoproteins constitute a premier model to dissect how specific and dynamic interactions in multisubunit membrane protein complexes can control deep-seated conformational rearrangements. However, individual residues that determine reciprocal specificity of the viral attachment and fusion (F) proteins have not been identified. We have developed an assay based on a pair of canine distemper virus (CDV) F proteins (strains Onderstepoort (ODP) and Lederle) that share ~95% identity but differ in their ability to form functional complexes with the measles virus (MV) attachment protein (H). Characterization of CDV F chimeras and mutagenesis reveals four residues in CDV F-ODP (positions 164, 219, 233, and 317) required for productive interaction with MV H. Mutating these residues to the Lederle type disrupts triggering of F-ODP by MV H without affecting functionality when co-expressed with CDV H. Co-immunoprecipitation shows a stronger physical interaction of F-ODP than F-Lederle with MV H. Mutagenesis of MV F highlights the MV residues homologous to CDV F residues 233 and 317 as determinants for physical glycoprotein interaction and fusion activity under homotypic conditions. In assay reversal, the introduction of sections of the CDV H stalk into MV H shows a five-residue fragment (residues 110–114) to mediate specificity for CDV F-Lederle. All of the MV H stalk chimeras are surface-expressed, show hemadsorption activity, and trigger MV F. Combining the five-residue H chimera with the CDV F-ODP quadruple mutant partially restores activity, indicating that the residues identified in either glycoprotein contribute interdependently to the formation of functional complexes. Their localization in structural models of F and H suggests that placement in particular of F residue 233 in close proximity to the 110–114 region of H is structurally conceivable.

Paramyxoviruses are enveloped nonsegmented negative strand RNA viruses. For all members of the subfamily paramyxovirinae, viral entry into target cells requires the concerted action of two envelope glycoproteins. The attachment protein (H, HN, or G depending on the genus) mediates receptor binding and is thought to trigger conformational rearrangements in the metastable F protein, which ultimately results in membrane fusion (1–4).

Ample structural information is available for both glycoproteins; the fusion protein ectodomain has been crystallized in both the metastable prefusion (3), and the final post-fusion (5, 6) conformation and partial structures of the ectodomain of the attachment protein have been solved for multiple paramyxovirinae including MV[2] (7–10). Identifying individual residues in each glycoprotein that are critical for the formation of functional fusion complexes and thus adding functional information to the available structural data has emerged as a central question in understanding the molecular mechanisms of paramyxovirus entry.

The F protein, a type I membrane protein, forms a noncovalently linked homotrimer. In its active form, each subunit of the trimer consists of a membrane-embedded F_1 and a disulfide-linked extracellular F_2 domain (11–14). A stabilized human parainfluenzavirus type 5 (hPIV5) F ectodomain has been reported to fold into a globular head structure that is attached through a helical stalk formed by membrane-proximal heptad repeat (HR)-B domains to the transmembrane domains (3). This is considered the prefusion conformation and is in contrast to structures of the nonstabilized Newcastle disease virus (6) and hPIV3 (5) F ectodomains, which show a distal head, a widening neck, and an extended helical stalk composed of the extended N-terminal HR-A coiled-coil. Transition to the latter from the prefusion conformation thus requires deep-seated conformational changes.

Crystal structures of the globular head domains of different paramyxovirinae attachment proteins have revealed the typical six-blade propeller fold of sialidase structures (7–10). Hemagglutinin-neuraminidase (HN) attachment proteins are indeed found on paramyxoviruses that enter cells through binding to sialic acid (11). However, viruses of the genera henipavirus (15–17) and morbillivirus recognize proteinaceous receptors (CD46 and/or SLAM/CD150w for MV (18–23)), and their attachment proteins lack neuraminidase activity. MV H has crystallized as homodimer (7, 8), but for some paramyxovirinae attachment proteins the formation of homotetramers consisting of dimers of dimers has additionally been demonstrated (9, 10, 24, 25). Stalk domains connect the transmembrane anchors of each subunit to the head domains.

* This work was supported, in whole or in part, by National Institutes of Health Grants AI056179 and AI071002 (to R. K. P.). The costs of publication of this article were defrayed in part by the payment of page charges. This article must therefore be hereby marked "*advertisement*" in accordance with 18 U.S.C. Section 1734 solely to indicate this fact.

[S] The on-line version of this article (available at http://www.jbc.org) contains supplemental methods and supplemental Figs. S1 and S2.

[1] To whom correspondence should be addressed: 2015 Uppergate Dr., Ste. 520, Emory University, Atlanta, GA 30322. Fax: 404-727-9223; E-mail: rplempe@emory.edu.

[2] The abbreviations used are: MV, measles virus; CDV, canine distemper virus; ODP, strain Onderstepoort; hPIV, human parainfluenzavirus; HR, heptad repeat; HN, hemagglutinin-neuraminidase; RT, reverse transcription; PBS, phosphate-buffered saline; H, hemagglutinin.

Both glycoprotein oligomers are considered to engage in specific protein-protein interactions with each other, because heterotypic glycoprotein pairs are typically unable to mediate membrane fusion (11, 12, 26) and do not co-precipitate (27). For paramyxovirus HN proteins, several studies have shown the stalk region to determine specificity for different F proteins, suggesting that F-interacting residues may reside in this region (28–33). However, the applicability of this finding to morbillivirus H is unknown.

Limited data are available regarding individual residues or microdomains in F that are required for productive interaction with the attachment protein. This reflects that the generation of F chimeras derived from different members of the paramyxovirus family typically compromise F functionality. Peptides derived from the HR-B domain of Newcastle disease virus or Sendai virus F reportedly interact with soluble variants of Newcastle disease virus (34) or Sendai HN (35). Multiple domains were suggested to mediate the specificity of hPIV2 F for homologous HN (36). However, the relevance of these peptide interactions in the context of native, membrane-embedded glycoproteins and the role of individual F residues in the formation of functional fusion complexes are unclear (33, 34).

For morbilliviruses, functional heterotypic complexes were reported in some studies that assessed combinations of MV and CDV-derived glycoproteins, constituting one of the few exceptions to strictly homotypic interaction (37–39). However, another study reported that MV H cannot functionally replace CDV H in triggering CDV F (40). This discrepancy in results could be due to the individual expression systems employed, absence of the natural viral receptors in the cell lines used, which have since been determined, or differences in the strain origin of the glycoproteins analyzed. An implication of the latter would be that F proteins derived from some CDV or, possibly, MV strains might be able to productively interact with heterotypic H, whereas those from other strains may not. If correct, this opens a novel avenue for the identification of residues that mediate paramyxovirus glycoprotein specificity. Identity between F proteins derived from different CDV or MV strains typically far exceeds 90%, thus providing a very high likelihood that chimeras of F proteins originating from different strains will be functional and allow tracing of the phenotype to individual residues.

Through testing this hypothesis, we have identified a pair of CDV F proteins derived from different strains that drastically differ in their ability to functionally interact with MV H. F chimera construction has been backed up by directed mutagenesis to explore whether a minimal set of residues is identifiable that mediates CDV F specificity for MV H. The relevance of these findings for the productive interaction of homotypic MV F and H has been examined. In parallel, we have sought through assay reversal to identify specific residues in MV H that are responsible for selective triggering of the F strain variants. In a single system, this procedure has highlighted specific residues in both glycoproteins that contribute interdependently to the formation of functional fusion complexes. Mechanistic implications have been explored by locating identified residues in the three-dimensional context of structural models derived for each glycoprotein complex.

EXPERIMENTAL PROCEDURES

Cell Culture, Transfection, and Production of Virus Stocks—All of the cell lines were maintained at 37 °C and 5% CO_2 in Dulbecco's modified Eagle's medium supplemented with 10% fetal bovine serum. Vero (African green monkey kidney epithelial) cells (ATCC CCL-81) stably expressing human SLAM (Vero-SLAM cells (41)) or canine SLAM (Vero-dogSLAM cells (42)) and baby hamster kidney (BHK-21) cells stably expressing T7 polymerase (BSR-T7/5 (BHK-T7) cells (43)) were incubated at every third passage in the presence of G-418 (Geneticin) at a concentration of 100 μg/ml. Lipofectamine 2000 (Invitrogen) was used for cell transfections. To prepare stocks of the CDV strain Onderstepoort (ODP; a kind gift of S. Niewiesk) or CDV strain Lederle (ATCC VR-128), Vero-dogSLAM cells were infected at a multiplicity of infection of 0.001 plaque-forming units/cell and incubated at 37 °C. The cells were scraped in OPTIMEM (Invitrogen), virus was released by two freeze-thaw cycles, and titers were determined by 50% tissue culture infective dose ($TCID_{50}$) titration according to the Spearman-Karber method (44) as described (45). To prepare stocks of modified vaccinia virus Ankara expressing T7 polymerase (MVA-T7, (46), DF-1 cells (ATCC CRL-12203) were infected at an multiplicity of infection of 1.0 plaque-forming unit/cell, and cell-associated viral particles were harvested 40 h post-infection.

RT-PCR and Subcloning of MV and CDV Envelope Glycoproteins—Vero-SLAM cells were infected with MV-Ill (MVi/Illinois.USA/50.99, genotype D3), MV-Y22 (MVi/Yaounde.CAM/83, genotype B1), or MV-KS (MVi/Kansas.USA, genotype D3) (47), and Vero-dogSLAM cells were infected with CDV strain ODP or Lederle, respectively. Following RT-PCR and subcloning of F and H encoding open reading frames into TOPO 2.1 vectors (Invitrogen), MV coding sequences in the MV glycoprotein expression constructs pCG-F and pCG-H (48) were replaced with the newly isolated counterparts, such that promoter sequences and flanking noncoding regions are identical for all F or H constructs, respectively. This ensures equal expression conditions for all of the proteins examined in the study (see supplemental information for RT-PCR details). All of the final constructs were fully sequenced and functionality confirmed by co-transfection into Vero-dogSLAM cells.

Generation of Chimeric Constructs and Mutagenesis—CDV F chimeras were generated through digestion of pCG-CDV F-Lederle and pCG-CDV F-ODP plasmids with PacI and the specified enzyme followed by ligation of the appropriate fragments. BglII and KpnI sites were engineered into the CDV F constructs through site-directed mutagenesis using the QuikChange mutagenesis system (Stratagene). All other CDV and MV F variants harboring point mutations were generated through site-directed mutagenesis using appropriate primers and confirmed by DNA sequencing. MV/CDV H chimeras were generated through recombination PCR using the cDNA copy of the MV genome and pCG-CDV H-Lederle as templates (see supplemental information for details). All other MV H variants (constructs *VI–XIII* in Fig. 5*B*) were generated through site-directed mutagenesis using appropriate primers and confirmed by DNA sequencing.

Quantitative Cell-to-Cell Fusion Assay—To quantify fusion activity, an effector Vero cell population (2×10^5 cells/well) was co-transfected with 2 μg each of H and F expression plasmid, and target Vero-dogSLAM cells (2×10^5 cells/well) were transfected with 2 μg of the reporter plasmid encoding firefly luciferase under the control of the T7 promoter. Single transfections of plasmids encoding H (for F chimera studies) or F (for H chimera studies) served as controls. Two hours post-transfection, the effector cells were infected with MVA-T7 at an multiplicity of infection of 1.0 plaque-forming unit/cell. Following incubation for 12–16 h at 30 °C, the target cells were detached, washed, overlaid on the effector cells at a 1:1 ratio, and incubated at 37 °C. Three to six hours post-overlay, the cells were lysed using Bright Glo Lysis Buffer (Promega), and the luciferase activity was determined using a luminescence counter (PerkinElmer Life Sciences) and the Britelite reporter gene assay system (PerkinElmer Life Sciences). The arbitrary values of the instrument were analyzed by subtracting relative background provided by values of the controls, and these values were normalized against reference constructs indicated in the figure legends. On average, background values were <1% of values obtained for reference constructs. To determine the extent of differential triggering, the ratio of values obtained for homotypic *versus* heterotypic glycoprotein pairs was calculated.

Microscopy—Vero or Vero-dogSLAM cells (4×10^5 cells/well) were co-transfected with 2 μg each of H and F expression plasmid and photographed 7–15 h post-transfection using a Nikon DIAPHOT 200 inverted microscope. The pictures were taken at a magnification of 200× using a SPOT Insight camera and SPOT Advanced software.

Co-immunoprecipitation—BHK cells were transfected with 4 μg each of plasmid DNA encoding H and F variants as specified in the individual experiments. At 30 h post-transfection, the cells were washed five times with cold PBS and lysed in immunoprecipitation buffer (10 mM Hepes, pH 7.4, 50 mM sodium pyrophosphate, 50 mM sodium fluoride, 50 mM sodium chloride, 5 mM EDTA, 5 mM EGTA, 1% Triton X-100, protease inhibitors (Roche Applied Science), and 1 mM phenylmethylsulfonyl fluoride). Cleared lysates (20,000 × g; 60 min; 4 °C) were incubated with specific antibodies directed against an epitope in the MV H ectodomain (Chemicon) at 4 °C, followed by precipitation with immobilized protein G (Pierce) at 4 °C. The precipitates were washed three times each in buffer A (100 mM Tris, pH 7.6, 500 mM lithium chloride, 0.1% Triton X-100) and then buffer B (20 mM HEPES, pH 7.2, 2 mM EGTA, 10 mM magnesium chloride, 0.1% Triton X-100) followed by resuspension in urea buffer (200 mM Tris, pH 6.8, 8 M urea, 5% SDS, 0.1 mM EDTA, 0.03% bromphenol blue, 1.5% dithiothreitol). Denatured samples were fractionated on 10% SDS-polyacrylamide gels, blotted onto polyvinylidene difluoride membranes (Millipore), and subjected to chemiluminescence detection (Amersham Biosciences) using antisera directed against an epitope in the cytosolic F tail. For densitometric quantification of co-precipitated F_1, blots were developed using a VersaDoc digital imaging system (Bio-Rad), and the signals were quantified with the QuantityOne software package. For each construct, the amount of F_1 material present in cell lysates prior to precipitation served as an internal standard.

F Surface Expression: Surface Biotinylation—Vero cells were transfected with 4 μg of plasmid DNA encoding F constructs as indicated. After washing in cold PBS, the cells were incubated in PBS with 0.5 mg/ml sulfosuccinimidyl-2-(biotinamido)ethyl-1,3-dithiopropionate (Pierce) for 20 min at 4 °C, followed by washing and quenching for 10 min at 4 °C in Dulbecco's modified Eagle's medium. The samples were lysed in immunoprecipitation buffer, and the lysates were cleared by centrifugation for 20 min at 20,000 × *g* and 4 °C. Biotinylated proteins were adsorbed to Sepharose-coupled streptavidin (Amersham Biosciences) for 120 min at 4 °C, washed three times each as detailed above, and incubated in urea buffer for 25 min at 50 °C. The samples were then subjected to immunoblotting and densitometric analysis as described above.

H Surface Expression: Cell Imaging—Vero cells were transfected with 4 μg of plasmid DNA encoding H constructs as indicated. Five hours post-transfection, the cells were detached and reseeded in a clear-bottomed 96-well black plate (COSTAR 3603) at a density of 3×10^4 cells/well. After incubating overnight at 37 °C, the cells were decorated with specific antibodies directed against an epitope in the MV H ectodomain (kind gift of Paul A. Rota) in Dulbecco's modified Eagle's medium supplemented with 5% fetal bovine serum and washed three times with Dulbecco's modified Eagle's medium (1% fetal bovine serum) after 1 h of incubation at 37 °C. Subsequent to incubation with goat anti-mouse IRDye 800CW (LI-COR) antibodies in Dulbecco's modified Eagle's medium (5% fetal bovine serum), the cells were washed and analyzed using an Odyssey infrared imager (LI-COR).

Hemadsorption—Vero cells were transfected with 4 μg of plasmid DNA encoding MV H constructs as indicated and the hemadsorption activity determined 24 h post-transfection by their ability to adsorb African green monkey erythrocytes as described previously (49). Washed cell monolayers were incubated with a 4% suspension of erythrocytes in PBS at 37 °C for 30 min, followed by washing and 10 min of incubation at 37 °C. The adsorbed erythrocytes were lysed in 50 mM NH_4Cl, and the absorbance of cleared lysates was quantified at 540 nm. Background obtained from equally treated mock transfected cells was subtracted from sample values.

Molecular Modeling—A homology model of CDV F-ODP was generated on the basis of the coordinates reported for prefusion PIV5 F trimer (Protein Data Bank code 2B9B (3)). Primary sequence comparison using ClustalW revealed 26% identity and 59% similarity between CDV F and PIV5 F (the CDV F precursor sequence (residues 1–135) was excised). The homology between these sequences is similar to that observed between hPIV3 F and Newcastle disease virus F (50). X-ray crystal structures for both of the latter in the post-fusion state show very similar three-dimensional folds, despite a slight rotation in the interface of the HR-A coiled-coil and the DI-DII domains (5). It was thus expected that faithful models also of prefusion F could be achieved based on similar homologies. Support for this comes from a previously generated MV F model that permitted us to successful engineer stabilizing disulfide bridges into the prefusion trimer (51). The CDV-F model was constructed using Prime (52). Each subunit was individually built and then combined into a trimer, which was further refined by using the

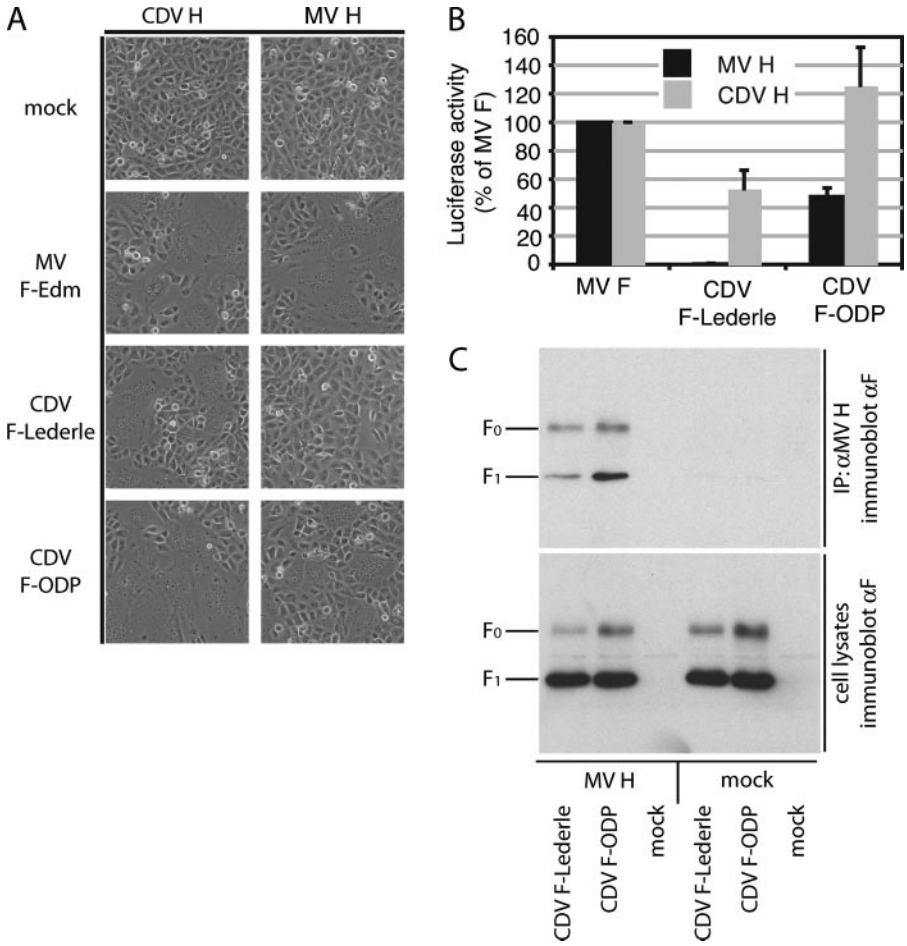

FIGURE 1. **CDV F-ODP but not CDV F-Lederle is triggered by MV H.** *A*, microphotographs of Vero-dogSLAM cells co-transfected with equal amounts of plasmid DNA encoding MV or CDV glycoproteins as specified. The cells were photographed at a magnification of 200× after incubation at 37 °C for seven to 11 h. Mock infected cells expressed only the H protein. *B*, quantification of cell-to-cell fusion activity using a firefly luciferase reporter-based fusion assay. The values reflect the average luciferase activities of at least three independent experiments ± S.D. per glycoprotein combination and are expressed as the percentages of activity measured for MV F and the respective H. *C*, CDV F glycoprotein variants show different strengths of interaction with MV H. Co-immunoprecipitation of CDV F-ODP and Lederle with MV H. The lysates of co-transfected cells were subjected to immunoprecipitation using specific antibodies directed against an epitope in the MV H ectodomain. Co-precipitated F (*upper panel*) was detected in comparison with F present in the lysates prior to precipitation (*lower panel*) by immunoblotting using a specific antiserum directed against an epitope in the cytosolic tail of CDV F.

Prime side chain prediction model on all residues. MV H modeling originated from x-ray crystal structures with Protein Data Bank codes 2ZB5 (8) and 2RKC (7). These structures, which show H as a homodimer, return information for the head domain (residues 154–607) but almost entirely lack the stalk domain (residues 58–153). Although the oligomeric state of native MV H has not formally been determined and may well resemble a tetramer (53) in accordance with other paramyxovirus attachment proteins (9, 10, 24, 25), homodimers are shown here consistent with the x-ray data. For residues 58–122 of the MV H stalk, secondary structure prediction by SSpro (54) return a helical fold for 81% of the residues. Given this strong prediction, these residues were mapped onto the helical structure of cortexillin I structure (Protein Data Bank code 1D7M) as a template. Using Prime, the MV-H residues were threaded so that the second intersubunit disulfide bridge between MV H cysteine residues at position 139 could form (55), whereas hydrophobic contacts at the contact points between the helices were maintained. Residues 1–57 covering the cytosolic tail and the transmembrane domain were not modeled. The model of the stalk peptides was attached to the MV H x-ray crystal structure, positioning the stalk perpendicular to the plane of the dimer. To relieve steric contacts, the structure was subjected to a molecular dynamics simulation using MACROMODEL (56) at 20 K for 500 femtoseconds (OPLS2005 force field, GB/SA water solvation, 0.5-femtosecond time step) with residues 144–164 allowed to move and the rest of the protein held as an aggregate. To juxtapose models of F and H, both structures were aligned at the termini of their transmembrane domains (residue 609 for CDV F and 58 for MV H, respectively).

RESULTS

In search of an assay for the identification of specific residues that engage in the formation of functional complexes of paramyxovirinae fusion and attachment proteins, we tested the hypothesis that heterotypic triggering of CDV or MV F by MV or CDV H is F strain-dependent. Genes encoding F proteins from MV strains MV-Ill, MV-Y22, or MV-KS (47), CDV strains ODP or Lederle, and CDV H-Lederle were isolated by RT-PCR and cloned under the control of the constitutive cytomegalovirus promoter. Vector backbones and noncoding regions flanking the open reading frames were made identical to pCG-F_{Edm} (48) for all F constructs and to pCG-H_{Edm} (48) for H constructs to maximize comparability.

MV H Efficiently Triggers CDV F-ODP but Not CDV F-Lederle—When Vero cells stably expressing dogSLAM (thus permissive for both CDV and MV-Edm (23, 42)) were co-transfected with these plasmids, we observed efficient cell-to-cell fusion resulting in syncytia formation for all homotypic glycoprotein pairs, confirming biological activity of the constructs (data not shown). Assessment of heterotypic combinations confirmed previous reports for F_{Edm} (38, 39) and revealed efficient heterotypic triggering also for wild type MV F variants F-Ill, F-Y22, F-KS, and CDV H-Lederle (data not shown). Importantly, however, a strong strain preference was found in the productive interaction of CDV F with MV H, with CDV F-ODP being triggered efficiently by MV H, whereas no fusion occurred upon co-transfection of cells with CDV F-Lederle and MV H (Fig. 1*A*). A firefly luciferase-based quantitative cell-to-

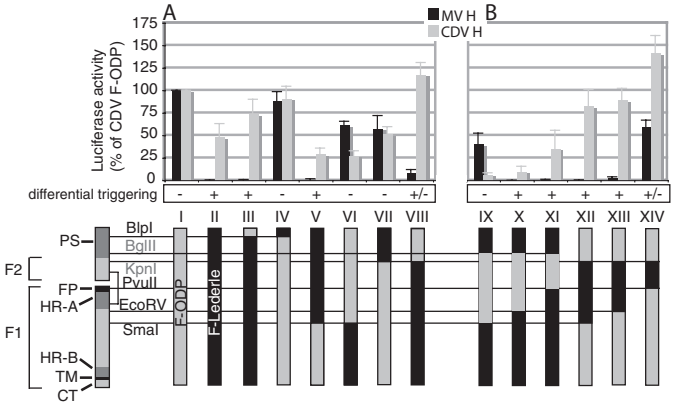

FIGURE 2. **Identification of a minimal domain responsible for productive interaction of CDV F variants with MV H.** *A*, quantification of cell-to-cell fusion activity of reciprocal chimeras between CDV F-ODP and Lederle upon co-transfection with MV H (*black bars*) or CDV H (*gray bars*) using the luciferase reporter-based fusion assay as outlined in Fig. 1*B*. The values were normalized for fusion activity observed upon co-transfection of cells with unmodified F-ODP and MV H or CDV H, respectively. The mean values ± S.D. of three independent experiments are shown, and the extent of differential triggering (based on the percentage of homotypic activity/percentage of heterotypic activity) is specified (see text for details). F constructs are schematized below the graph. The *black boxes* represent regions derived from F-Lederle, and the *gray boxes* represent F-ODP. The location of characteristic F protein domains, the site of the disulfide bridge linking the F_1 and F_2 subunits (*black line*), and the position of natural (BlpI, PvuII, EcoRV, and SmaI) and engineered (BglII and KpnI, in *gray*) restriction sites used for chimera generation are shown on the *left*. *PS*, N-terminal precursor sequence of CDV F; *FP*, fusion peptide; *HR-A*, N-terminal heptad repeat; *HR-B*, C-terminal heptad repeat; *TM*, transmembrane domain; *CT*, cytosolic tail. *B*, focused chimeras based on engineered restriction sites identify a domain in the N-terminal part of F-ODP (between restriction sites KpnI and EcoRV, construct XIII) to determine productive interaction of F-ODP with MV H. Quantification of fusion activity, calculation of differential triggering and color coding as described in *A*.

cell fusion assay confirmed these microscopic observations (Fig. 1*B*).

To test whether CDV F-Lederle is still capable of physically interacting with MV H, we adapted a co-immunoprecipitation assay that we have previously developed for homotypic MV glycoprotein interactions (45, 57). When F-ODP and F-Lederle were examined in this assay, both F variants were found to form hetero-oligomers with MV H. However, co-precipitation efficiency of F-ODP with MV H was substantially higher than that of F-Lederle (Fig. 1*C*). These findings reveal different degrees of heterotypic glycoprotein interaction and support our hypothesis that productive heterotypic interaction of CDV F with MV H depends on the strain background of the CDV F examined.

A Minimal Domain Required for Heterotypic Triggering of CDV F-ODP—F-Lederle and F-ODP share >95% protein identity. This makes it likely that chimeras derived from both proteins are fusion-competent, in contrast to heterotypic chimeras combining F proteins from different paramyxoviruses. To test this prediction, a series of reciprocal chimeras was generated using suitable restriction sites that are conserved in both CDV F genes (schematic in Fig. 2*B*, *constructs III–VIII*). When fusion activity of these constructs was determined, productive interaction of F-ODP with MV H was traced to an N-terminal region of F (Fig. 2*A*; see supplemental Fig. S1*A* for microphotographs), downstream from large parts of the N-terminal precursor sequence, which is unique to CDV F and reportedly proteolytically removed prior to F maturation (58). In addition to surface biotinylation to determine intracellular transport (supplemental Fig. S2*A*), quantification of fusion activity of these and all subsequent F constructs upon co-transfection with homotypic CDV H served as an internal standard for each individual construct (Fig. 2*A*, *gray bars*). The ratio of quantified fusion activity (% of reference F) upon co-expression of each F with homotypic *versus* heterotypic H was than calculated, and each construct was assigned to one of three categories of differential triggering: −, fusion under homotypic and heterotypic conditions, ratio 0.5–1.9; +/−, some syncytia detectable under heterotypic conditions, ratio 2.0–15; +, no syncytia detectable under heterotypic conditions, ratio >15) (Fig. 2*A*). This procedure ensures specific comparison of the ability of each F variant to engage in functional interaction with either H by minimizing the influence of variation in the overall fusogenicity of individual F chimeras.

To further narrow the domain responsible for differential triggering of the CDV F variants by MV H, silent mutations generating a BglII site at amino acid position 100 or a KpnI site at position 149 were introduced into the CDV F variants, and a second series of chimeras was produced. Transfer of an 861-bp (287-residue) BglII/SmaI fragment from F-ODP to F-Lederle generated an F-Lederle chimera that was more efficiently triggered by MV H than by CDV H itself (Fig. 2*B*). Further shortening of the transferred ODP fragment prevented the formation of active fusion complexes with MV H (constructs X and XI). However, fusion activity under homotypic conditions was substantially reduced for construct X, suggesting some incompatibility of these ODP fragments in the F-Lederle background. This was accentuated by our additional finding that an F-Lederle chimera harboring an ODP KpnI/SmaI fragment was fusion-incompetent under both homotypic and heterotypic conditions (data not shown).

In contrast, a much smaller 574-bp (191-residue) KpnI/EcoRV fragment spanning the C-terminal 73 amino acids of the F_2 subunit, the fusion peptide and the HR-A domain emerged as responsible for differential triggering when the complementary chimeras were generated in the F-ODP background. Introducing this region from F-Lederle into F-ODP resulted in an ODP chimera that entirely lost its ability to form functional fusion complexes with MV H, whereas, importantly, productive homotypic interaction with CDV H was fully maintained (Fig. 2*B*, *constructs XII* and *XIII*). Further shortening of this segment reduced the degree of differential triggering (Fig. 2*B*, *construct XIV*). Specific changes in this 191-residue domain between both CDV F variants are thus responsible for productive heterotypic triggering of F-ODP. These findings underscore the suitability of our assay to identify residues in F and likely also H that determine productive envelope glycoprotein interaction.

Four Point Mutations Disrupt Productive Interaction of F-ODP with MV H—The 191-amino acid domain harbors six residues that differ between F-Lederle and ODP (highlighted in *black* in the alignment shown in Fig. 3*A*). A single, rather conservative arginine *versus* lysine mutation at position 317 was detected in the area flanked in the coding sequence by the PvuII and EcoRV sites. Because our results have highlighted this mutation as a contributor to differential triggering of F-Lederle *versus* F-ODP with MV H (Fig. 2*B*, *constructs XIII* and *XIV*), this

residue was first changed to lysine by directed mutagenesis in the F-ODP background. Although it did not fully disrupt activation of F-ODP by MV H, the R317K mutation alone reduced heterotypic triggering of F-ODP (Fig. 3*B*). Combining Lys^{317} with changes at any three of the five remaining positions (residues 164, 219, or 233) further reduced heterotypic triggering, whereas residues 159 and 178 did not enhance or even partially reverted the phenotype. The greatest effect, closely resembling

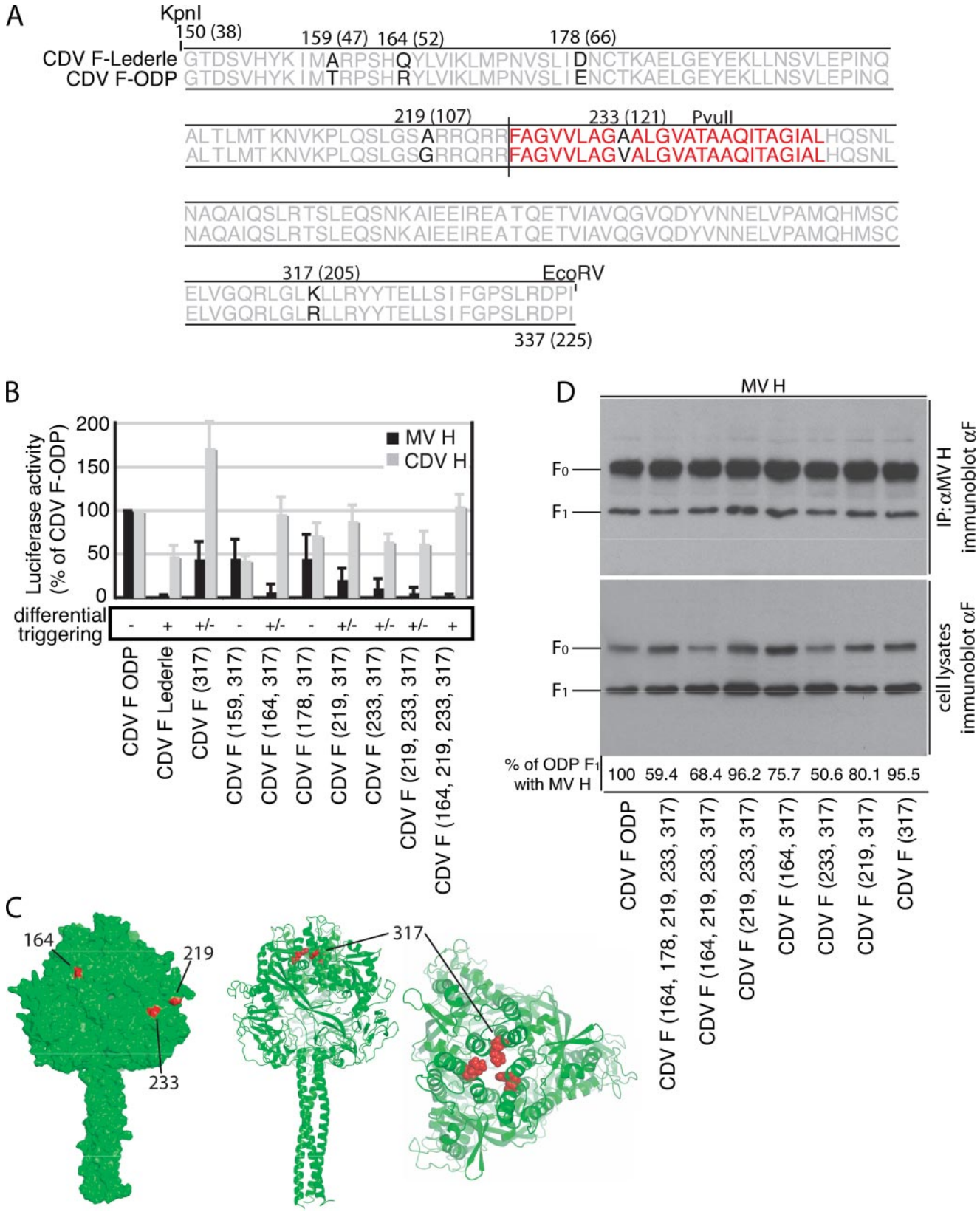

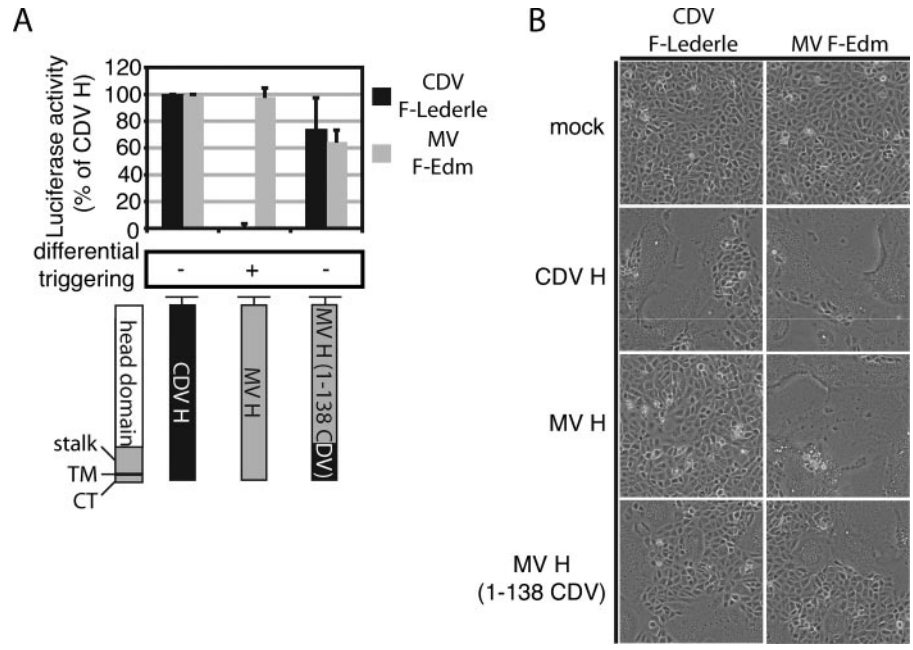

FIGURE 4. **Residues in an MV H N-terminal domain are determinants for F specificity.** *A*, quantification of fusion activity upon activation of CDV F-Lederle or MV F with CDV H, MV H, or an MV/CDV H chimera specified in the schematic below the graph. The activity was determined as outlined before (Fig. 1*A*), and the values are expressed as a percentage of activity observed for either CDV F-Lederle or MV F co-expressed with CDV H. The averages of three independent experiments ± S.D. and the extent of differential triggering are shown. *Stalk*, membrane-proximal part of the H ectodomain (up to residue 139); *TM*, transmembrane domain; *CT*, cytosolic tail. *B*, microphotographs of Vero-dogSLAM cells co-transfected with the constructs outlined in *A*. The pictures were taken 9.5 h post-transfection at a magnification of 200×. Mock transfected cells received only F-encoding plasmid.

values observed before for chimera XIII (Fig. 2*A*), was observed when residues 164, 219, 233, and 317 were changed in conjunction (Fig. 3*B*; see supplemental Figs. S1*B* for microphotographs and S2*B* for surface expression).

To locate these residues in the three-dimensional context of the prefusion F trimer, we generated a structural model of CDV F on the basis of the coordinates reported for the prefusion F of the related hPIV5 (3). The side chains of residues 164, 219, and 233 are each predicted to be surface-exposed, whereas residue 317 is completely buried in the prefusion trimer (Fig. 3*C*).

The contribution of the different mutations to the strength of glycoprotein interaction was assessed biochemically by co-precipitation of the individual F-ODP variants with MV H. Co-precipitation efficiency of mature, fusion-competent F_1 was somewhat reduced as compared with unmodified F-ODP, indicating a lowered strength of physical glycoprotein interaction (Fig. 3*D*). However, no linear trend emerged, suggesting that changes in physical and functional interaction of these ODP mutants with MV H are not directly proportional.

These findings indicate that four discrete point mutations modulate the physical interaction of F-ODP with MV H and govern the ability of both proteins to form functional fusion complexes.

Assay Reversal Demonstrates That the Nature of the H Stalk Domain Determines Productive Interaction of MV H with CDV F-Lederle—We next examined whether the assay is expandable to the attachment protein and thus suitable to identify residues in morbillivirus H that are responsible for differential triggering of the CDV F-Lederle and ODP chimeras. We have previously demonstrated that covalent MV H dimerization is mediated by tandem intersubunit disulfide bridges that engage cysteines at positions 139 and 154, respectively (55). These cysteines are conserved in CDV H, leading to the hypothesis that a fragment comprising the cytosolic tail, transmembrane anchor, and stem domain up to the first disulfide bridge may be transferable between CDV and MV H as a modular unit without losing functionality.

To test this hypothesis and assess whether CDV F-specificity of MV H is associated with this N-terminal fragment or downstream domains, we generated an MV H mutant in which the N-terminal 139-residue fragment is derived from CDV H. Quantification of cell-to-cell fusion activity and microscopic assessment upon co-expression of this H construct with MV F or CDV F-Lederle demonstrated that the construct is equally capable of efficiently triggering either F (Fig. 4).

These findings indicate that residues located in the MV H ectodomain downstream of the N-terminal stalk region are not involved in differential F triggering in our assay. They are fully consistent with previous studies that have implicated stalk domains of the HN proteins of related paramyxoviruses in mediating F specificity (28–33). Our data extend these studies to morbillivirus H.

FIGURE 3. **Four point mutations disrupt productive interaction of CDV F-ODP with MV H.** *A*, amino acid sequence alignment of the identified fragment between the KpnI and EcoRV sites of F-Lederle and ODP. The *black letters* indicate residues that differ between the strains. The fusion peptide (*red*) and the relative position of the PvuII site are shown. A *vertical line* marks the furin cleavage site. *B*, quantitative comparison of fusion activity of individual F-ODP point mutants. The values are expressed as percentages of fusion activity observed upon co-transfection with unmodified F-ODP and either MV or CDV H. The averages of four experiments ± S.D. and the extent of differential triggering are shown. *C*, visualization of the identified residues in a structural model of the prefusion CDV F-ODP trimer. In the *left panel*, all four residues (164, 219, 233, and 317) are highlighted in *red*. Residues 164, 219, and 233 are predicted to be surface-exposed; residue 317 is predicted to be completely buried in the trimer (visible only in the ribbon models; *center panel*, side view; *right panel*, top view). For clarity, residues 164, 219, and 233 are not highlighted in the ribbon models. *D*, co-immunoprecipitation of selected F-ODP mutant constructs with MV H reveals a limited reduction in co-precipitation efficiency as compared with unmodified F-ODP. The experimental conditions were the same as described for Fig. 1*C*. The values below the blot represent averages of densitometric quantification of co-precipitated F_1 material from two independent experiments. They are corrected for the amount of F_1 material present in cell lysates prior to precipitation, which serves as internal standard (*lower panel*), and are expressed as percentage of co-precipitated CDV F_1-ODP.

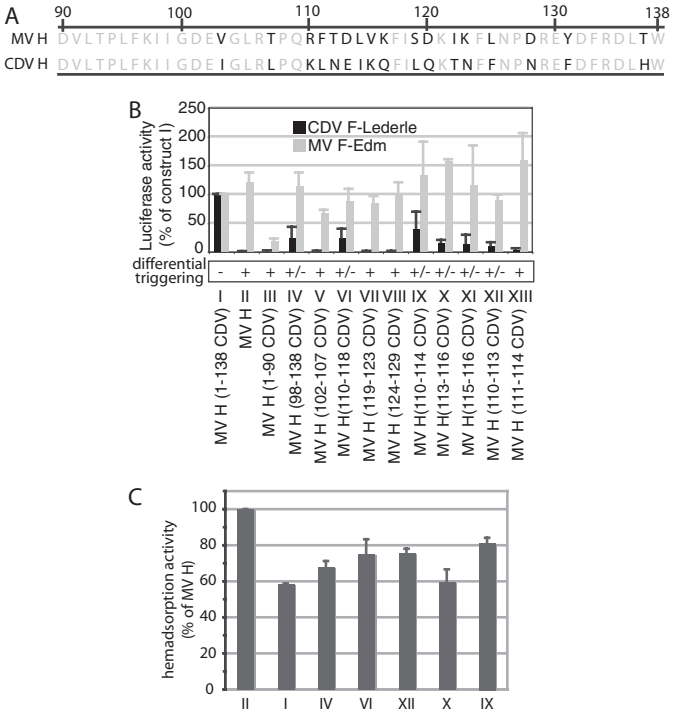

FIGURE 5. **Transferring a linear domain of five CDV residues into the H stalk renders MV H capable of activating CDV F-Lederle.** *A*, amino acid sequence alignment of a 49 residue-stretch in the H stalk domain identified in *B* to mediate specificity of MV H for CDV F-Lederle. The *bold letters* indicate residues that differ between the H variants. *B*, a minimal CDV H-derived microdomain spanning residues 110–114 is required for CDV F-Lederle activation by MV H variants. Quantitative fusion assays of cells co-transfected with CDV F-Lederle or MV F and MV H variants as specified below the graph. The values are expressed as the percentages of activity upon co-transfection of CDV F-Lederle or MV F with chimeric MV H (1–138 CDV) covering the area under investigation. The averages of three independent experiments ± S.D. and the extent of differential triggering are shown. *C*, hemadsorption activity of selected H constructs. *Roman numerals* specify the H variants introduced in *B*. The values are averages of two independent experiments; the *error bars* represent the range observed.

A Five-residue Fragment in the MV H Stalk Determines Specificity for F-Lederle—To test whether individual residues in MV H can be identified that contribute to F-Lederle activation, a conserved region downstream of residue 90 (Fig. 5*A*) was chosen as a base to systematically narrow the 139-amino acid fragment.

Through recombination PCR, two additional MV H chimeras were generated that harbor either CDV residues 1–90 (cytosolic tail, transmembrane domain, N-terminal residues of the stalk domain) or 98–138 (C-terminal residues of the stalk domain up to the first disulfide bridge). Microscopic assessment and quantification of homotypic and heterotypic F triggering revealed that only the latter H construct was capable of productively interacting with F-Lederle (Fig. 5*B*, *constructs III* and *IV*, and supplemental Fig. S1*C*). Further differentiation of the 41-residue fragment (position 98–138) through recombination PCR backed up by directed mutagenesis highlighted a linear five-residue fragment (residues 110–114) to be accountable for the degree of F-Lederle activation observed for H construct IV (Fig. 5*B*, *construct IX*). Although this chimera, MV H (110–114 CDV), activates F-Lederle only ~40% as efficiently as MV H (1–138 CDV), no other linear domain in the 138-residue stretch was found to contribute to F-Lederle specificity when assessed individually. Further shortening of this fragment reduced fusion activity upon co-expression with F-Lederle (Fig. 5*B*, *constructs X–XII*).

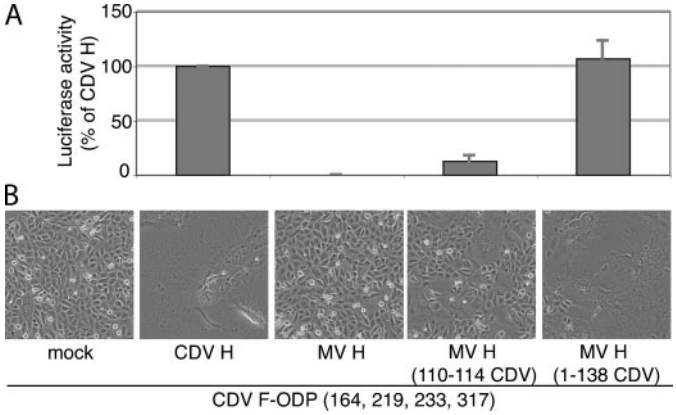

FIGURE 6. **Residues identified in F and H act interdependently.** Quantitative (*A*) and qualitative (*B*) assessment of fusion activity of cells co-transfected with the CDV F-ODP (residues 164, 219, 233, and 317) variant introduced in Fig. 3*B* and CDV H, MV H, or chimeras derived thereof as specified. The quantification results are expressed as percentages of activity observed for cells co-expressing CDV F-ODP (residues 164, 219, 233, and 317) and homotypic CDV H. The averages of three independent experiments ± S.D. are shown. The microphotographs were taken 13 h post-transfection at a magnification of 200×.

All but one of the H chimeras were capable of triggering homotypic MV F (fusion activity upon co-expression with MV F >50% of standard MV H), suggesting that other functions such as surface expression and receptor binding are largely intact. However, several residues in region 84–105 of the MV H stalk were shown previously to modulate hemadsorption activity (49). We thus assessed for several constructs surface expression by whole cell surface imaging (supplemental Fig. S2*C*) and hemadsorption activity as a surrogate for receptor binding (Fig. 5*C*). Both assays returned values of ≥60% that of unmodified MV H, which is fully consistent with the results of the fusion assays.

These data demonstrate that residues in the extracellular H stalk domain determine whether a functional interaction can be established between MV H and CDV F-Lederle. Changing these to the homologous CDV sequence in the MV H background has little impact on hemadsorption activity or surface expression.

Co-expression of F and H Chimeras Reveals Interdependence of the Identified Residues in Productive Glycoprotein Interaction—To assess whether the residues individually identified in F and H act interdependently and thus determine reciprocal glycoprotein specificity, we co-expressed the strictly CDV H-dependent F-ODP (164 219 233 317) variant with different MV H chimeras capable of triggering F-Lederle and examined fusion activities quantitatively and qualitatively (Fig. 6). Control transfections reconfirmed productive interaction of this F variant with CDV H and the complete absence of its triggering by MV H. The presence of the N-terminal 138-amino acid domain of CDV H fully restored the ability of MV H to productively interact with this F-ODP variant, and co-expression with MV H (110–114 CDV) resulted in some fusion activity, albeit to a lesser degree than observed with MV H (1–138 CDV). The latter is not limited to F-ODP (164 219 233 317) but

rather continues the trend observed initially when the ability of this H chimera to productively interact with F-Lederle was examined (Fig. 5*B*).

These data confirm that productive interaction is restored when mutations of residues 164, 219, 233, and 317 in F-ODP are combined with changing the 110–114 stretch in MV H. These residues thus act interdependently in determining reciprocal glycoprotein specificity.

Role of Identified F Residues in Homotypic Fusion—To assess the importance of F residues 164, 219, 233, and 317 for the formation of productive fusion complexes under homotypic conditions, we mutated the homologous residues (positions 52, 107, 121, and 205) individually in the MV F background. Changes at either position 52 or position 107 had virtually no effect on F fusion activities (112% ± 12% of unmodified MV F for F-Q52A and 98% ± 9% of unmodified MV F for F-S107A (Fig. 7*A*)) or surface expression (Fig. 7*B*).

In contrast, a rather conservative alanine to leucine change at MV F position 121, which maintains the hydrophobic-aliphatic character of the side chain, resulted in nearly complete intracellular retention of the mutant protein (Fig. 7*B*). Despite the block in intracellular transport, cell-to-cell fusion was ~21% of unmodified MV F (Fig. 7*A*), indicating that the very small fraction of surface-expressed material is sufficient to mediate detectable activity. The opposite phenotype was observed when alanine 121 was changed to lysine. Plasma membrane levels of MV F_1-A121K are similar to those of unmodified F_1, indicating folding into a transport-competent form and successful proteolytic maturation (Fig. 7*B*). Upon co-expression with MV H, however, essentially no fusion activity (0.2% ± 0.1% of unmodified F) could be detected in quantitative fusion assays (Fig. 7*A*; for microphotographs see supplemental Fig. S1*D*).

For MV F residue 205, a conservative change of the lysine at this position to histidine or glutamine, which preserved the basic respectively polar character of the side chain, reduced fusion activity by 19% (Gln) to 79% (His) (Fig. 7*A*). A more drastic change at this position (K205A) fully abrogated fusion activity. Mutation F-R205A and to a lesser degree F-R205H also reduce intracellular transport competence (Fig. 7*B*). However, F_1 plasma membrane steady-state levels, in particular of F_1-R205H, far exceeded those observed for F_1-A121L, indicating that the reduction in surface expression alone cannot account for the loss in fusion activity.

In contrast to residue 205, the structural model of MV F predicts residue 121 exposed at the surface of the prefusion trimer. To test whether mutation of this residue to lysine physically affects homotypic interaction, co-immunoprecipitation with MV H was employed. The F-A121K variant returned an approximate 81% reduction in co-precipitation efficiency with MV H as compared with unmodified F (Fig. 7*C*), highlighting this residue as a determinant for physical glycoprotein interaction. Because the amount of fusion-competent matured F_1-A121L is below the detection limit, the leucine variant could not be assessed in this assay.

These results demonstrate that of the four candidate residues identified in the heterotypic assay, MV F residues 121 and 205 are determinants for the strength of homotypic MV glycoprotein interaction (residue 121) and the extent of fusion activity.

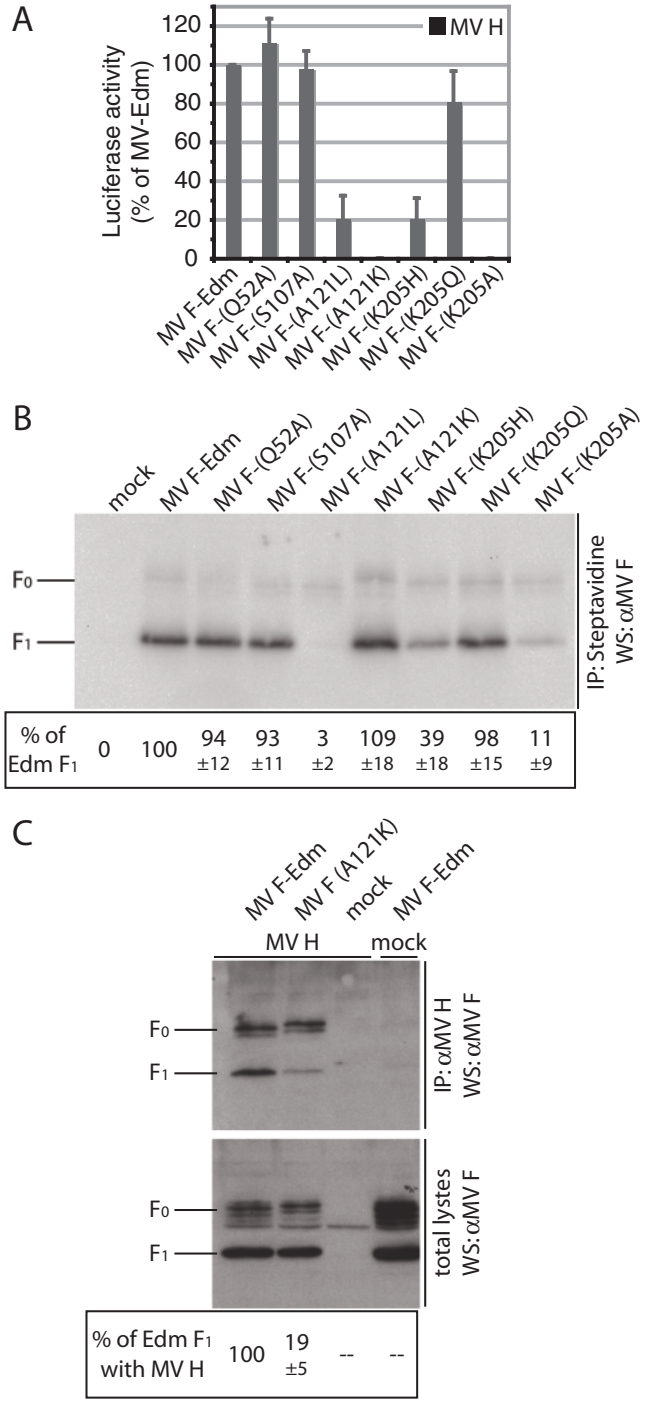

FIGURE 7. **Role of the identified F residues in fusion under homotypic conditions.** *A*, quantification of cell-to-cell fusion activity of cells co-transfected with MV H and MV F-Edm variants carrying point mutations at positions homologous to CDV F residue 164, 219, 233, or 317. The results are expressed as percentages of activity observed for cells co-expressing MV H and F-Edm. The averages of at least three independent experiments ± S.D. are shown. *B*, surface biotinylation to determine plasma membrane steady-state levels of MV F-Edm variants examined in *A*. The values below the blot represent averages of densitometric quantification of matured F_1 material from three independent experiments ± S.D., expressed as a percentage of standard Edm F_1. *C*, an A121K mutation in MV F-Edm reduces the efficiency of co-precipitation by homotypic MV H. The experimental procedures are the same as described for Fig. 1*C*. The values below the blot represent averages of densitometric quantification of co-precipitated F_1 material from three independent experiments ± S.D.

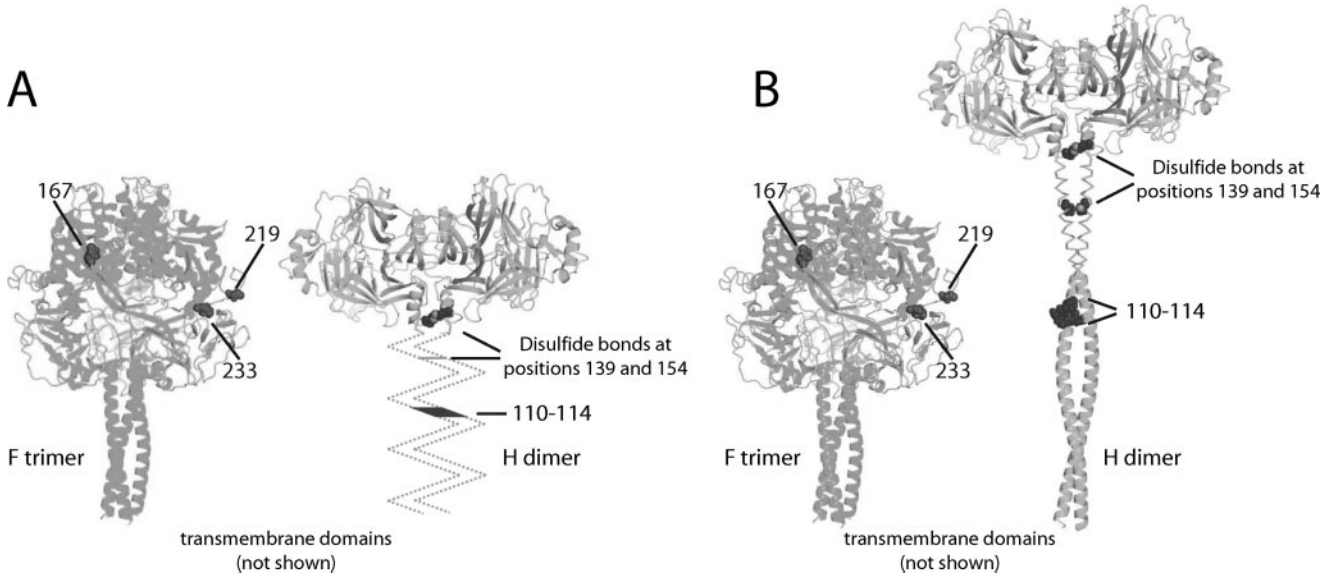

FIGURE 8. **Two possible hypotheses of envelope glycoprotein alignment.** H stalk domains are represented in unknown (*A*) or helical (residues 58–122) (*B*) conformation. The helical H stalk places H residues 110–114 and F residues 233 and 219 at the lateral face of the prefusion CDV F trimer at an equal distance above the viral envelope, making short range interactions structurally conceivable (*B*). The ribbon models of the glycoprotein oligomers are aligned at their transmembrane domains. Helical modeling of H stalk residues 58–122 is based on the predictions of SSpro (54) (81% helical). Cysteines 139 and 154 engaging in intersubunit disulfide bonds (55) are shown.

DISCUSSION

With the availability of substantial structural information on paramyxovirus envelope glycoproteins, understanding the molecular mechanism of functional glycoprotein interaction has gained momentum (1, 59). Multiple studies have employed chimeric envelope proteins as tools to identify microdomains that mediate reciprocal glycoprotein specificity under heterotypic conditions (28–31). Although generally successful for the attachment protein, this approach has met severe obstacles in the case of paramyxovirus F.

Toward overcoming these, the key advantage of our approach is that we have identified two F proteins of different CDV strains that share >95% identity but are differentially triggered by MV H. In our experimental setting, the productive heterotypic interaction between CDV F-ODP and MV H-Edm glycoproteins previously described (38, 39) was confirmed. Consistent with a different report (40), however, this apparently is not a general phenomenon because we found CDV F-Lederle incapable of forming functional fusion complexes with MV H-Edm. Given that the CDV strain analyzed by Wild *et al.* (40) was not specified, we cannot determine at present whether CDV F-Lederle was examined both by Wild and colleagues and in our work. However, although certainly of interest, this question is irrelevant for the goals of our mechanistic study.

Construction of reciprocal CDV F chimeras consistently highlighted an N-terminal domain that, when shuttled between both F variants, results in gain-of-function in the case of F-Lederle (triggering by MV H) or loss-of-function in the case of F-ODP (triggering by MV H is blocked). However, some of the second generation F-Lederle chimeras were fusion inactive even under homotypic conditions, indicating the incompatibility of some of the transferred F-ODP-specific residues with the F-Lederle background. This underscores the challenges in uncovering residues that govern the complex dynamic changes in the F trimer during fusion. F-ODP shows a higher degree of tolerance for F-Lederle specific changes. Mutation of four residues (CDV F positions 164, 219, 233, and 317) to the F-Lederle type fully disrupts activation of F-ODP by MV H but does not compromise fusion activity under homotypic conditions. Rather than impairing overall F activity, these mutations thus selectively block the functional interaction of F-ODP with MV H.

Several studies have indicated a role for the stalk domain of the paramyxovirus hemagglutinin-neuraminidase protein in specific, productive interaction with F (29–33). Our results for morbillivirus H provide clear evidence that this observation extends to paramyxovirus attachment proteins that recognize protein receptors and thus likely constitutes a general theme in paramyxovirus glycoprotein interaction. The identification of H and F residues involved in mediating glycoprotein specificity in a single system opens a unique possibility to verify results through combination of glycoprotein variants with altered specificity ranges. The MV H chimera harboring the CDV H stalk domain indeed effectively activates the F-ODP (positions 164, 219, 233, and 317) quadruple mutant that is fully restricted to homotypic CDV H. This demonstrates that the H and F microdomains identified are interdependent in their effect on productive interaction and, consequently, are reciprocal determinants of envelope protein specificity.

To place these findings in the context of the available structural information, we have highlighted the identified residues in a side-by-side comparison of two possible alignments of the H and F structures (Fig. 8). In these models, the H and F stem domains are considered to extend perpendicularly from the viral membrane. This orients the receptor-binding sites in the H head domains (53, 60) toward the target membrane rather than backwards toward the viral envelope. It is also in accord

with the crystal structure of stabilized prefusion hPIV5 F, which did not reveal a kink between the GCNt domain, mimicking the transmembrane domains and the HR-B stalks (3). Fig. 8*A* does not assign a specific secondary structure to the H stalk, whereas Fig. 8*B* shows the membrane-proximal residues 58–122 as α-helix. The latter is based on strong secondary structure predictions by SSpro (54), which posits 81% of these residues helical and thus generates confidence of helical character (61).

Strikingly, when the models are aligned at the transmembrane-spanning domains, F residues 219 and 233 are predicted to be positioned at approximately the same level above the viral envelope as the 110–114 microdomain in the helical H stalk (Fig. 8*B*). Although these residues could contribute to glycoprotein specificity through long range effects, this observation alternatively makes direct contacts structurally conceivable. The latter would likewise provide a straightforward explanation for the results of previous studies showing a specific role of the paramyxovirus HN protein stalk in functional and physical interaction with F (29–33).

Direct contact of the H stalk with the prefusion F head would mandate positioning of the globular H head domain above the F trimer to avoid steric interference and thus require an extended H stalk as suggested in Fig. 8*B*. Interestingly, an early electron microscopy study suggests prominent spikes on the measles virus surface to correspond to the attachment protein, whereas the fusion function was considered to reside closer to the virus membrane (62). Consistent with this, a recent electron cryomicroscopy analysis of hPIV5 particles concludes that defined glycoprotein spikes, previously observed in electron microscopy studies of paramyxovirus particles (11), correspond in the case of F to the post-fusion conformation and thus represent a product of premature F refolding (63). Defined spikes corresponding to prefusion F were not detected in this cryo-electron microscopy study, but a dense corona-like surface layer was found, compatible with a tight packaging of the glycoprotein complexes and overshadowing of the F trimers by H as implied by the hypothetical model shown in Fig. 8*B*.

Our experiments demonstrate that mutation of the MV F residue 121 (the homologue of CDV F residue 233) causes a substantial reduction in physical interaction of matured F with homotypic MV H. Residue 121 is part of the fusion peptide, which is propelled toward the target membrane during F refolding (1, 59). Its predicted position on a lateral corner of the prefusion trimer renders it accessible for MV H. Increasing hydrophilicity of the fusion peptide could interfere with its association with target membranes, blocking fusion, if refolding of the F-A121K variant can be triggered. Importantly, however, our co-precipitation experiments assess the physical interaction of proteolytically matured F with H in the absence of fusion. In contrast to matured F, the mutation had very little effect on the intracellular interaction of immature F_0 with H. This likely reflects that paramyxovirus F reportedly is subject to some conformational change upon cleavage (64), which may affect the interaction with the attachment protein. Only matured F is fusion-competent, however, and thus able to form functional fusion complexes with H. Importantly, the physical homotypic interaction of these matured glycoproteins prior to fusion is impaired by the A121K mutation.

Although the positioning of CDV F residue 317 (MV F residue 205) in the model precludes direct contact with H, residues at these positions are important contributors to F triggering in the homotypic setting of MV glycoprotein complexes. The charged side chains of CDV F 317R are predicted to form a ring-like structure near the top of the prefusion F trimer. Repulsion between these positive charges could modulate the conformational stability of metastable prefusion F. Thus, residues at this position in the top of the F head appear ideally located to influence the initiation of F conformational rearrangements through long range effects.

In contrast to MV F residues 121 and 205, mutating residues 52 and 107 (corresponding to CDV F residues 164 and 219) has only marginal effects on fusion activity under homotypic conditions. The functional importance of these residues is thus restricted to heterotypic glycoprotein complexes, arguing against engagement in short range interactions in homotypic complexes. In particular for F residue 52, the predicted positioning in the structural model is fully consistent with this view.

Additional microdomains may contribute to mediating glycoprotein specificity but may be conserved across the MV and CDV proteins examined and thus not be picked up by our assay. Directed mutagenesis guided by a model of envelope glycoprotein interaction based on the current data will contribute to elucidating the nature of these domains and could lead to a interaction model with residue level accuracy.

Acknowledgments—We thank J.-J. Yoon and D. Chawla for help, P. A. Rota and S. Niewiesk for antibodies and viruses, and A. L. Hammond for critical reading of the manuscript.

REFERENCES

1. Lamb, R. A., Paterson, R. G., and Jardetzky, T. S. (2006) *Virology* **344,** 30–37
2. Colman, P. M., and Lawrence, M. C. (2003) *Nat. Rev. Mol. Cell. Biol.* **4,** 309–319
3. Yin, H. S., Wen, X., Paterson, R. G., Lamb, R. A., and Jardetzky, T. S. (2006) *Nature* **439,** 38–44
4. Kielian, M., and Jungerwirth, S. (1990) *Mol. Biol. Med.* **7,** 17–31
5. Yin, H. S., Paterson, R. G., Wen, X., Lamb, R. A., and Jardetzky, T. S. (2005) *Proc. Natl. Acad. Sci. U. S. A.* **102,** 9288–9293
6. Chen, L., Gorman, J. J., McKimm-Breschkin, J., Lawrence, L. J., Tulloch, P. A., Smith, B. J., Colman, P. M., and Lawrence, M. C. (2001) *Structure* (*Camb.*) **9,** 255–266
7. Colf, L. A., Juo, Z. S., and Garcia, K. C. (2007) *Nat. Struct. Mol. Biol.* **14,** 1227–1228
8. Hashiguchi, T., Kajikawa, M., Maita, N., Takeda, M., Kuroki, K., Sasaki, K., Kohda, D., Yanagi, Y., and Maenaka, K. (2007) *Proc. Natl. Acad. Sci. U. S. A.* **104,** 19535–19540
9. Crennell, S., Takimoto, T., Portner, A., and Taylor, G. (2000) *Nat. Struct. Biol.* **7,** 1068–1074
10. Yuan, P., Thompson, T. B., Wurzburg, B. A., Paterson, R. G., Lamb, R. A., and Jardetzky, T. S. (2005) *Structure* **13,** 803–815
11. Lamb, R. A., and Parks, G. D. (2007) in *Fields Virology* (Knipe, D. M., and Howley, P. M., eds) 5th Ed., pp. 1449–1496, Wolters Kluwer/Lippincott Williams & Wilkins, Philadelphia, PA
12. Dutch, R. E., Jardetzky, T. S., and Lamb, R. A. (2000) *Biosci. Rep.* **20,** 597–612
13. Plemper, R. K., Hammond, A. L., and Cattaneo, R. (2001) *J. Biol. Chem.* **276,** 44239–44246
14. Scheid, A., and Choppin, P. W. (1974) *Virology* **57,** 475–490
15. Bonaparte, M. I., Dimitrov, A. S., Bossart, K. N., Crameri, G., Mungall,

B. A., Bishop, K. A., Choudhry, V., Dimitrov, D. S., Wang, L. F., Eaton, B. T., and Broder, C. C. (2005) *Proc. Natl. Acad. Sci. U. S. A.* **102,** 10652–10657
16. Negrete, O. A., Levroney, E. L., Aguilar, H. C., Bertolotti-Ciarlet, A., Nazarian, R., Tajyar, S., and Lee, B. (2005) *Nature* **436,** 401–405
17. Negrete, O. A., Wolf, M. C., Aguilar, H. C., Enterlein, S., Wang, W., Muhlberger, E., Su, S. V., Bertolotti-Ciarlet, A., Flick, R., and Lee, B. (2006) *PLoS Pathogens* **2,** 78–86
18. Dorig, R. E., Marcil, A., Chopra, A., and Richardson, C. D. (1993) *Cell* **75,** 295–305
19. Naniche, D., Varior-Krishnan, G., Cervoni, F., Wild, T. F., Rossi, B., Rabourdin-Combe, C., and Gerlier, D. (1993) *J. Virol.* **67,** 6025–6032
20. Manchester, M., Eto, D. S., Valsamakis, A., Liton, P. B., Fernandez-Munoz, R., Rota, P. A., Bellini, W. J., Forthal, D. N., and Oldstone, M. B. (2000) *J. Virol.* **74,** 3967–3974
21. Oldstone, M. B., Homann, D., Lewicki, H., and Stevenson, D. (2002) *Virology* **299,** 162–163
22. Tatsuo, H., Ono, N., Tanaka, K., and Yanagi, Y. (2000) *Nature* **406,** 893–897
23. Tatsuo, H., Ono, N., and Yanagi, Y. (2001) *J. Virol.* **75,** 5842–5850
24. Lawrence, M. C., Borg, N. A., Streltsov, V. A., Pilling, P. A., Epa, V. C., Varghese, J. N., McKimm-Breschkin, J. L., and Colman, P. M. (2004) *J. Mol. Biol.* **335,** 1343–1357
25. Thompson, S. D., Laver, W. G., Murti, K. G., and Portner, A. (1988) *J. Virol.* **62,** 4653–4660
26. Hu, X. L., Ray, R., and Compans, R. W. (1992) *J. Virol.* **66,** 1528–1534
27. Yao, Q., Hu, X., and Compans, R. W. (1997) *J. Virol.* **71,** 650–656
28. Deng, R., Wang, Z., Mirza, A. M., and Iorio, R. M. (1995) *Virology* **209,** 457–469
29. Tanabayashi, K., and Compans, R. W. (1996) *J. Virol.* **70,** 6112–6118
30. Tsurudome, M., Kawano, M., Yuasa, T., Tabata, N., Nishio, M., Komada, H., and Ito, Y. (1995) *Virology* **213,** 190–203
31. Deng, R., Mirza, A. M., Mahon, P. J., and Iorio, R. M. (1997) *Arch. Virol. Suppl.* **13,** 115–130
32. Wang, Z., Mirza, A. M., Li, J., Mahon, P. J., and Iorio, R. M. (2004) *Virus Res.* **99,** 177–185
33. Melanson, V. R., and Iorio, R. M. (2006) *J. Virol.* **80,** 623–633
34. Gravel, K. A., and Morrison, T. G. (2003) *J. Virol.* **77,** 11040–11049
35. Tomasi, M., Pasti, C., Manfrinato, C., Dallocchio, F., and Bellini, T. (2003) *FEBS Lett.* **536,** 56–60
36. Tsurudome, M., Ito, M., Nishio, M., Kawano, M., Okamoto, K., Kusagawa, S., Komada, H., and Ito, Y. (1998) *J. Gen. Virol.* **79,** 279–289
37. Nussbaum, O., Broder, C. C., Moss, B., Stern, L. B., Rozenblatt, S., and Berger, E. A. (1995) *J. Virol.* **69,** 3341–3349
38. von Messling, V., Zimmer, G., Herrler, G., Haas, L., and Cattaneo, R. (2001) *J. Virol.* **75,** 6418–6427
39. Stern, L. B., Greenberg, M., Gershoni, J. M., and Rozenblatt, S. (1995) *J. Virol.* **69,** 1661–1668
40. Wild, T. F., Fayolle, J., Beauverger, P., and Buckland, R. (1994) *J. Virol.* **68,** 7546–7548
41. Ono, N., Tatsuo, H., Hidaka, Y., Aoki, T., Minagawa, H., and Yanagi, Y. (2001) *J. Virol.* **75,** 4399–4401
42. Seki, F., Ono, N., Yamaguchi, R., and Yanagi, Y. (2003) *J. Virol.* **77,** 9943–9950
43. Buchholz, U. J., Finke, S., and Conzelmann, K. K. (1999) *J. Virol.* **73,** 251–259
44. Spearman, C. (1908) *Br. J. Phsychol.* **2,** 227–242
45. Plemper, R. K., Hammond, A. L., Gerlier, D., Fielding, A. K., and Cattaneo, R. (2002) *J. Virol.* **76,** 5051–5061
46. Sutter, G., Ohlmann, M., and Erfle, V. (1995) *FEBS Lett.* **371,** 9–12
47. Plemper, R. K., Doyle, J., Sun, A., Prussia, A., Cheng, L. T., Rota, P. A., Liotta, D. C., Snyder, J. P., and Compans, R. W. (2005) *Antimicrob. Agents Chemother.* **49,** 3755–3761
48. Cathomen, T., Naim, H. Y., and Cattaneo, R. (1998) *J. Virol.* **72,** 1224–1234
49. Corey, E. A., and Iorio, R. M. (2007) *J. Virol.* **81,** 9900–9910
50. Smith, B. J., Lawrence, M. C., and Colman, P. M. (2002) *Protein Eng.* **15,** 365–371
51. Lee, J. K., Prussia, A., Snyder, J. P., and Plemper, R. K. (2007) *J. Virol.* **81,** 8821–8826
52. *Prime* (2005) Schrödinger, LLC, New York, NY
53. Griffin, D. E. (2007) in *Fields Virology* (Knipe, D. M., and Howley, P. M., eds) 5th Ed., pp. 1551–1585, Wolters Kluwer/Lippincott Williams & Wilkins, Philadelphia, PA
54. Cheng, J., Randall, A. Z., Sweredoski, M. J., and Baldi, P. (2005) *Nucleic Acids Res.* **33,** 72–76
55. Plemper, R. K., Hammond, A. L., and Cattaneo, R. (2000) *J. Virol.* **74,** 6485–6493
56. *MacroModel* (2005) version 9.1 Schrödinger, LLC, New York, NY
57. Plemper, R. K., and Compans, R. W. (2003) *J. Virol.* **77,** 4181–4190
58. von Messling, V., and Cattaneo, R. (2002) *J. Virol.* **76,** 4172–4180
59. Lamb, R. A., and Jardetzky, T. S. (2007) *Curr. Opin. Struct. Biol.* **17,** 427–436
60. Vongpunsawad, S., Oezgun, N., Braun, W., and Cattaneo, R. (2004) *J. Virol.* **78,** 302–313
61. Pollastri, G., Przybylski, D., Rost, B., and Baldi, P. (2002) *Proteins* **47,** 228–235
62. Armstrong, M. A., Fraser, K. B., Dermott, E., and Shirodaria, P. V. (1982) *J. Gen. Virol.* **59,** 187–192
63. Ludwig, K., Schade, B., Bottcher, C., Korte, T., Ohlwein, N., Baljinnyam, B., Veit, M., and Herrmann, A. (2008) *J. Virol.* **82,** 3775–3781
64. Dutch, R. E., Hagglund, R. N., Nagel, M. A., Paterson, R. G., and Lamb, R. A. (2001) *Virology* **281,** 138–150